PNAS RESEARCH ARTICLE | MEDICAL SCIENCES OPEN ACCESS

ALK signaling primes the DNA damage response sensitizing ALK-driven neuroblastoma to therapeutic ATR inhibition

Marcus Borenäs[a,1], Ganesh Umapathy[a,1], Dan E. Lind[a,1], Wei-Yun Lai[a,1], Jikui Guan[a,1], Joel Johansson[a], Eva Jennische[a], Alexander Schmidt[b], Yeshwant Kurhe[a], Jonatan L. Gabre[a,c], Agata Aniszewska[a], Anneli Strömberg[d], Mats Bemark[d,e], Michael N. Hall[f], Jimmy Van den Eynden[c,2], Bengt Hallberg[a,2], and Ruth H. Palmer[a,3]

Edited by James Cleaver, University of California, San Francisco, CA; received September 1, 2023; accepted November 28, 2023

High-risk neuroblastoma (NB) is a significant clinical challenge. MYCN and Anaplastic Lymphoma Kinase (ALK), which are often involved in high-risk NB, lead to increased replication stress in cancer cells, suggesting therapeutic strategies. We previously identified an ATR (ataxia telangiectasia and Rad3-related)/ALK inhibitor (ATRi/ALKi) combination as such a strategy in two independent genetically modified mouse NB models. Here, we identify an underlying molecular mechanism, in which ALK signaling leads to phosphorylation of ATR and CHK1, supporting an effective DNA damage response. The importance of ALK inhibition is supported by mouse data, in which ATRi monotreatment resulted in a robust initial response, but subsequent relapse, in contrast to a 14-d ALKi/ATRi combination treatment that resulted in a robust and sustained response. Finally, we show that the remarkable response to the 14-d combined ATR/ALK inhibition protocol reflects a robust differentiation response, reprogramming tumor cells to a neuronal/Schwann cell lineage identity. Our results identify an ability of ATR inhibition to promote NB differentiation and underscore the importance of further exploring combined ALK/ATR inhibition in NB, particularly in high-risk patient groups with oncogene-induced replication stress.

ALK | neuroblastoma | ATR | elimusertib | lorlatinib

High-risk neuroblastoma (NB) is a childhood cancer that currently presents a clinical challenge, reflected in the fact that NB accounts for 15% of all pediatric tumor related deaths (1). Although aggressive NB initially responds to treatment, later relapses exhibit poor prognosis and survival rates of around 35% (2, 3). For this reason, extensive efforts are being made to identify more effective therapeutic options. The relative paucity of mutations in NB has made it challenging to identify targetable therapeutic options. Genes with increased somatic mutation frequencies in NB include *ALK*, *PTPN11*, *ATRX,* and *NRAS*, where ALK can be therapeutically targeted by small molecule tyrosine kinase inhibitors (TKIs) (4–8). Amplification of the *MYCN* transcription factor is observed in approximately 20% of NB and is an important predictive factor that is currently therapeutically intractable (9, 10). Although lacking in mutations, NB exhibits numerous somatic chromosomal lesions, including deletion of regions of chromosome 1p, 11q, and gain of 2p, 17q, as well as aneuploidy, that provide important prognostic information (6).

Increased genome instability, commonly seen in tumors, leads to the engagement of DNA damage sensor systems (11). The DNA damage response (DDR) employs members of the PI3-kinase-related protein kinase (PIKK) family, such as the ataxia telangiectasia and Rad3-related (ATR) and ataxia-telangiectasia mutated (ATM), to ensure DNA integrity (12). ATR also has an important role in cell survival in response to replication stress by preventing replication origin firing and reducing the number of active forks, maintaining stability of stalled replication forks, facilitating repair, and promoting replication restart (12, 13). ATR was recently identified as a potent therapeutic target in preclinical models of NB (14–17), and we demonstrated that combined inhibition of ATR (with elimusertib) and ALK (with lorlatinib) results in a complete ablation of tumors in ALK-driven NB genetically engineered mouse models (GEMMs). While ATR is a downstream target of ALK signaling in NB cells (14), the underlying molecular mechanisms involved in the dramatic responses to ALK/ATR inhibition in ALK-driven models of NB (14) have been elusive.

Here, we demonstrate the superiority of ALKi/ATRi combination therapy over monotherapy in ALK-driven NB GEMMs and show that this combined effect is explained by ALK priming the DDR through phosphorylation of ATR on Ser 435 and CHK1 on Ser 280. We further identify a robust differentiation response in tumors treated with ATR inhibitors. Taken together, these results strongly motivate the continued exploration of ATR/ALK inhibition as a potentially therapeutically effective approach in NB.

Significance

Anaplastic Lymphoma Kinase (ALK) was identified as an oncogene in neuroblastoma (NB) in 2008 and together with MYCN drives aggressive NB in both human patients and genetically modified mouse models. These tumors are sensitive to ALK tyrosine kinase inhibitor (TKI) therapy, which is employed clinically. Here, we show that combined ALK/ATR (ataxia telangiectasia and Rad3-related) inhibition is superior to monotherapy, identifying a role for ALK signaling in supporting the DNA damage response. This therapeutic approach results in a robust tumor differentiation response. The long-term relapse-free response in response to ALK/ATR inhibition requires the cyclic GMP-AMP synthase/stimulator of IFN genes (cGAS/STING) pathway, as mice treated with cGAS/STING inhibitor relapse in response to treatment. These data identify this ALK/ATR inhibitor combination as a strong therapeutic strategy for treatment of ALK-positive NB patients.

The authors declare no competing interest.

This article is a PNAS Direct Submission.

[1]M.B., G.U., D.E.L., W.-Y.L., and J.G. contributed equally to this work.

[2]J.V.d.E. and B.H. contributed equally to this work.

[3]To whom correspondence may be addressed. Email: ruth.palmer@gu.se.

This article contains supporting information online at https://www.pnas.org/lookup/suppl/doi:10.1073/pnas.2315242121/-/DCSupplemental.

Published December 28, 2023.

Results

Combined ATR/ALK Inhibition Is More Effective than Monotreatment in ALK-Driven Mouse NB Models. In previous work, we reported a robust and sustained complete response to combinatorial ALK/ATR inhibitor treatment in two ALK-driven GEMM of NB (14). In these models, monotreatment with the ALK TKI lorlatinib results in tumor responses that are not sustained on drug removal (14, 18, 19). To better understand this, we compared 14-d ATRi monotreatment with the ALKi/ATRi combinatorial regime in *Alk-F1178S;Th-MYCN* (19) mouse NB tumors. Tumor-bearing mice were treated with a 14-d regime that either combined elimusertib together with lorlatinib (3 d (days 1-3) elimusertib twice daily, 4 d (days 4-7) lorlatinib twice daily, 3 d (days 8-10) combination, 4 d (days 11-14) lorlatinib) or employed elimusertib alone (3 d (days 1-3) elimusertib twice daily, 4 d off treatment, 3 d (days 8-10) elimusertib, 4 d off treatment) (Fig. 1 *A* and *B*). Tumor volumes were monitored with ultrasound at 4, 7, 11 and 14 d during the 14-d treatment. As previously reported, all mice tolerated the treatment regime with no noticeable side effects (14). No tumors were detected at day 14 after combined ALKi/ATRi treatment (Fig. 1*C*). Elimusertib monotherapy resulted in a significant reduction in tumor size but did not result in a complete resolution of tumor material at day 14. Mice were observed over time without any further therapeutic interventions and monitored regularly for tumor development. Remarkably, 14-d combinatorial treatment (elimusertib/lorlatinib) resulted in a sustained complete response as we have previously reported (14). In contrast, elimusertib monotreatment resulted in tumor relapse, with 50% of treated mice relapsing within 43 d after treatment cessation compared with 0% relapse at this time in mice treated with the elimusertib/lorlatinib combination [log-rank (Mantel–Cox) test, $P < 0.05$; log-rank test; Fig. 1*D*].

ALK Signaling Primes the DDR in NB Cells. Our earlier analysis of ALK TKI treatment in NB cells identified ATR in the ALK regulated phosphoproteome (20). To reveal the effect of ALK signaling on ATR and the DDR, we performed a phosphoproteomics analysis of NB cells (NB1) stimulated with 1 µg/mL ALKAL2 ligand for 15 min. This confirmed ATR as an ALK target, with ALKAL2 stimulation leading to increased phosphorylation of Ser435 (log2FC = 1.754; $P = 1.4 \times 10^{-5}$), a growth factor stimulated ATR site reported to regulate ATR activity. ALK stimulation also induced CHK1 phosphorylation at Ser280 (log2FC = 1.56; $P = 2.6 \times 10^{-4}$). Of note, this ALKAL2 stimulated CHK1 phosphorylation was not at the ATR S/TQ target Ser345 that is paradoxically increased in response to CHK1 inhibition by LY2603618 (21) (Fig. 2*A*). Further, inhibition with lorlatinib decreased CHK1 Ser280 phosphorylation (log2FC = −1.31; $P = 6.8 \times 10^{-6}$). We confirmed CHK1 phosphorylation on Ser280 in response to ALKAL2 stimulation in two independent NB cell lines, CLB-BAR and NB1 (Fig. 2*A*). Phosphorylation of CHK1 S280 was independent of ATR, as addition of elimusertib did not block phosphorylation in response to ALK activation. Conversely, inhibition of ALK with lorlatinib in ALK-driven CLB-BAR, CLB-GE and CLB-GAR NB cell lines resulted in decreased pCHK1 S280 (Fig. 2*B*). It has been reported that phosphorylation of CHK1 on Ser280 regulates CHK1 localization (22). To investigate this, NB cells were stimulated with ALKAL2, and cytoplasmic and nuclear fractions were immunoblotted for pCHK1 S280. A robust increase in pCHK1 S280 on ALK stimulation was detected in both cytoplasmic and nuclear fractions, although no significant difference in the total amount of CHK1 in the nuclear fraction was detected (Fig. 2*C*). Since phosphorylation of CHK1 on S280 has been reported to accelerate CHK1 activation and prime the DDR, we investigated the effect of ALK inhibition on the DDR. ALK-driven CLB-BAR, CLB-GE, and CLB-GAR NB cells were treated with lorlatinib for 24 h and phosphorylation of H2A.X on S139 monitored as readout of DNA damage. Indeed, ALK inhibition increased pH2A.X in all three cell lines (Fig. 2*D*). These results suggest that ALK inhibition decreases the cellular DDR, resulting in DNA damage. This was confirmed by analysis of 276 genes that have been associated with the DDR (23) (further referred to as the DDR signature) in previously published RNA-Seq datasets from NB cell lines treated with lorlatinib (19, 20). Lorlatinib treatment for 6 h or more resulted in significant reduction of the DDR signature in ALK-dependent CLB-BAR, CLB-GE, and NB1 NB cell lines but not in IMR32 and SKNAS that are not dependent on

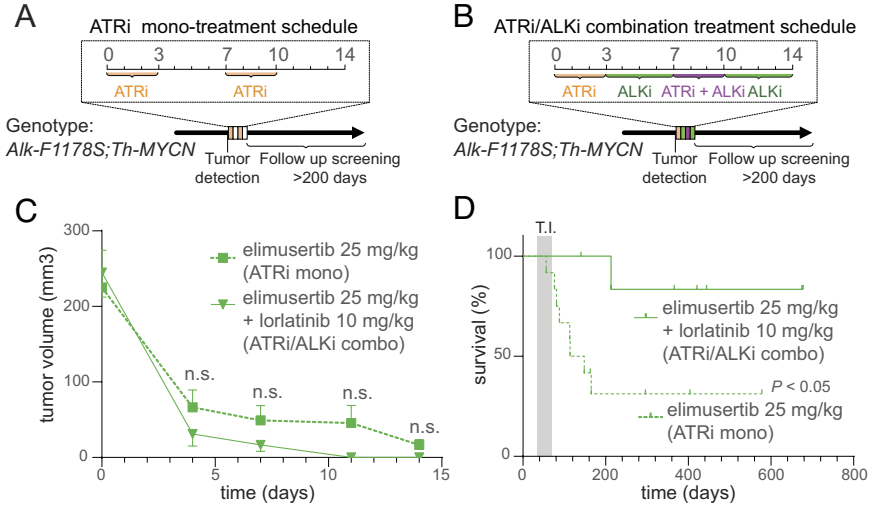

Fig. 1. ALK inhibition enhances tumor response and progression-free survival in mice treated with ATR inhibitors. (*A*) Monotreatment regimen for Alk/MYCN-driven GEMM tumors. Tumor-bearing mice were treated with 25 mg/kg ATRi (elimusertib) for 3 d; after this, a 4-d pause from treatment was followed by an additional 3 d of elimusertib. (*B*) In the combination regimen, the initial monotreatment with ATRi was followed by 10 mg/kg lorlatinib for 11 d, with the addition of ATRi at days 8 to 10. All treatments were given orally twice daily. (*C*) Tumor volume measured by ultrasound over 14 d. Data are presented as mean ± SEM. n.s. = not significant. (*D*) Survival (from birth) of *Alk-F1178S;Th-MYCN* mice treated with elimusertib monotreatment (n = 12) compared with elimusertib/lorlatinib combination treatment (n = 7). $P < 0.05$; log-rank (Mantel–Cox) test. The shaded area indicates tumor incidence (T.I.) range.

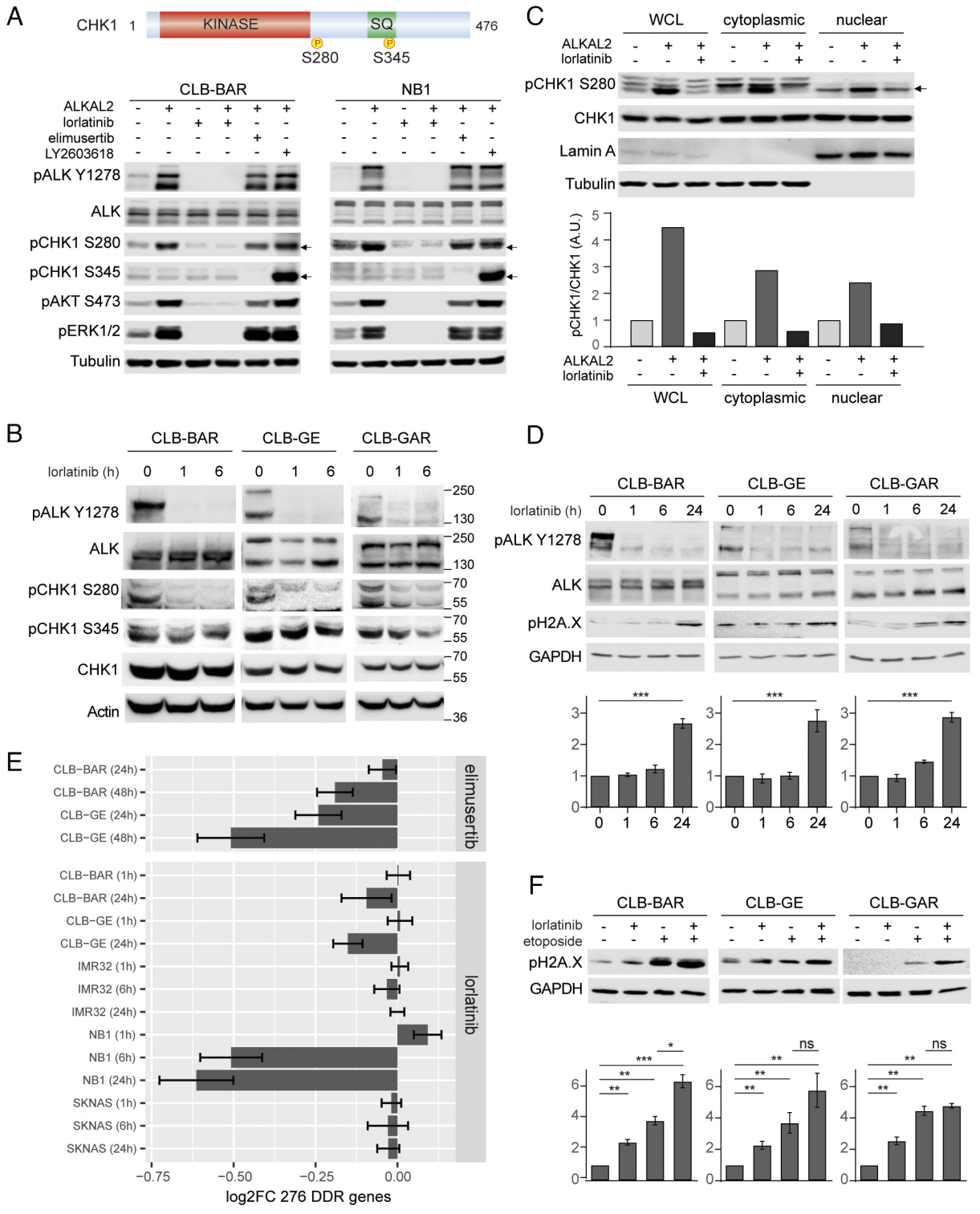

Fig. 2. ALK signaling activity drives phosphorylation of CHK1 on S280. (*A*) ALK-driven CLB-BAR and NB1 cells were treated with different inhibitors (2 h) or 1 μg/mL ALKAL2 ligand (0.5 h) alone or in combination as indicated. Inhibitors employed were the ALK inhibitor lorlatinib (20 nM), the ATR inhibitor elimusertib (100 nM), and the CHK1 inhibitor LY2603618 (1 μM). Lysates were immunoblotted for pALK (Y1278), ALK, pCHK1 (S280), pCHK1 (S345), pAKT (S473), pERK1/2 (T202/Y204), and Tubulin. Serine sites S280 (downstream of ALK) and S345 (downstream of ATR) are highlighted schematically in CHK1 (*Top*). CHK1 kinase domain (in red) and regulatory SQ domain (SQ, in green). Arrowheads indicate pCHK1 (S280) and pCHK1 (S345). (*B*) ALK-positive CLB-BAR, CLB-GE, and CLB-GAR NB cells treated with lorlatinib (30 nM) for 0, 1, and 6 h. Lysates were immunoblotted for pALK (Y1278), ALK, pCHK1 (S280), pCHK1 (S345), CHK1, and Actin. (*C*) Lysates and cytoplasmic or nuclear extracts of CLB-BAR cells treated with 1 μg/mL ALKAL2 ligand alone or in combination with lorlatinib were immunoblotted for pCHK1 (S280), CHK1, Lamin A (nuclear marker) and β-tubulin (cytoplasmic marker). The arrowhead indicates pCHK1 (S280). Quantification of pCHK1/CHK1 ratios normalized to controls is shown below. (*D*) ALK-positive CLB-BAR, CLB-GE, and CLB-GAR NB cells were treated with lorlatinib (30 nM) at different time points, as indicated. Lysates were immunoblotted for ALK, pALK (Y1278), and p-H2A.X (S139). GAPDH was employed as loading control. n = 3 biologically independent experiments. Unpaired *t* test; ***$P < 0.001$. (*E*) Bar plot showing RNA-Seq-based log2FC values (mean ± 95% CI) of 276 genes involved in the DDR for different NB cell lines and drug treatments as indicated. Data were derived from five previously published studies (14, 19, 20, 24, 25) with DDR genes as defined by Knijnenburg et al. (23). CLB-BAR, CLB-GE, and NB1 are ALK-dependent lines. IMR32 cells express ALK but are not ALK-dependent for cell growth. SKNAS (*NRAS, Q61K*) cells lack detectable ALK expression and are ALK-independent (26, 27). (*F*) ALK-positive CLB-BAR, CLB-GE, and CLB-GAR NB cells were treated with lorlatinib (30 nM) or etoposide (500 nM), either alone or in combination for 24 h. DNA damage was monitored by immunoblotting of p-H2A.X (S139). GAPDH was employed as loading control. n = 3 biologically independent experiments. Unpaired *t* test; ns, not significant; *$P < 0.05$; **$P < 0.01$; ***$P < 0.001$.

ALK for growth (Fig. 2*E*). Similar DDR reductions were observed for other ALK inhibitors and other ALK-driven NB cell lines for which RNA-Seq data are publicly available (*SI Appendix*, Fig. S1). Taken together, our data suggest that ALK signaling modulates the DDR in ALK-driven NB cells. To test this, we next treated ALK-driven CLB-BAR, CLB-GE, and CLB-GAR NB cells with lorlatinib and the DNA damaging topoisomerase II inhibitor etoposide, either alone or in combination for 24 h (Fig. 2*F*). Treatment with etoposide alone resulted in increased pH2A.X, that was further increased on ALK inhibition, although this was only significant in CLB-BAR cells. Taken together, these data suggest a molecular mechanism by which ALK inhibition is able to increase the efficacy of ATR treatment.

Elimusertib Is More Potent than Ceralasertib in NB Cell Lines. Pediatric clinical phase I/II trials with elimusertib have recently been initiated (clinicaltrials.gov; NCT05071209), but no clinical data have been reported. Another ATR inhibitor, ceralasertib, was recently employed in combination with the Aurora-A kinase inhibitor alisertib in MYCN-driven NB models (15). We therefore compared ceralasertib with elimusertib in our experimental setup. While ALK-driven CLB-BAR and CLB-GE cell lines were sensitive to both ATR inhibitors, elimusertib displayed higher potency [IC50s of 67.51 ± 10.23 nM for CLB-BAR and 49.68 ± 8.42 nM for CLB-GE, in agreement with our previous findings (14)] than ceralasertib (IC50s of 480.1 ± 9.56 nM for CLB-BAR and 813 ± 11.06 nM for CLB-GE) (Fig. 3*A*), agreeing with previously published analyses (17). To confirm these findings, we compared treatment of CLB-BAR and CLB-GE NB cells with either 50 nM elimusertib, 50 nM ceralasertib, or 1 μM ceralasertib for 24 h, immunoblotting for pATR, ATR, pATM, ATM, pCHK1, CHK1, PARP/cl.PARP, p53, and pH2A.X (Fig. 3*B*). As expected, 50 nM elimusertib inhibited phosphorylation of ATR S428 and downstream pCHK1 S345 and resulted in increased cleaved PARP, p53, and pH2A.X. In contrast, 50 nM ceralasertib was insufficient for ATR inhibition, and 1 μM was required to effectively inhibit ATR signaling and the DDR.

High levels of ceralasertib were also required to perturb ATR regulation of the S/G2 checkpoint that controls mitotic entry (28) (Fig. 3*C*). The ATR targets pFOXM1 (T600) and pCHK1 (S345) were monitored in CLB-GE cells synchronized by thymidine block and levels of pFOXM1 and pCHK1 monitored in the presence or absence of elimusertib (50 nM) or ceralasertib (50 nM or 1 μM) for 6 h after thymidine release (Fig. 3*C* and *SI Appendix*, Fig. S2). In agreement with previous findings (14), enhanced pFOXM1, prominent in metaphase, was observed in CLB-GE cells released from thymidine block in response to ATR inhibition by either 50 nM elimusertib or 1 μM ceralasertib, but not at 50 nM ceralasertib (Fig. 3*C*). Thus, similar effects were noted for both elimusertib and ceralasertib, although inhibition by ceralasertib required 20-fold higher amounts compared with elimusertib.

Phosphoproteomics Profiling of Ceralasertib in NB Cells. We previously characterized the effect of elimusertib mediated ATR inhibition on the NB cell phosphoproteome, identifying a strong compensatory activation of ATM that resulted in increased S/TQ target phosphorylation in response to treatment (14). Although a previous phosphoproteomics analysis employed AZ20, from which ceralasertib is derived (29), there is no information on the effect of either AZ20 or ceralasertib on the NB phosphoproteome.

To better understand the different effects of elimusertib and ceralasertib, we compared the phosphoproteome of CLB-BAR cells treated with either 50 nM ceralasertib, 1 μM ceralasertib, or 50 nM elimusertib for 6 h after release from thymidine block. A total of 11,026 phosphosites (9,655 Ser, 1,351 Thr, and 20 Tyr) were identified in 3,244 different proteins (Dataset S1). Differential phosphorylation (DP) was observed at 618 sites (521 phosphorylated and 97 dephosphorylated) in 368 proteins in response to elimusertib treatment (log2FC threshold 0.3 at 5% FDR; Fig. 4*A*), in good agreement with our previous analysis (14). Elimusertib induced dephosphorylation of ATR T1989 and its downstream target CHK1 S317 and a compensatory phosphorylation of ATM S1981 and its downstream targets CHK2 at S379 and S260. We observed a similar compensation at DNA-dependent protein kinase (DNAPK) sites S3205, S2612, and S2624. These responses were highly similar at high concentrations of ceralasertib (1 μM; 276 DP sites; Pearson's $R = 0.88$), with the notable exception of ATR T1989, which responded weakly to ceralasertib as compared to elimusertib (log2FC = −0.42 versus log2FC = −1.74, respectively; Fig. 4 *A* and *C*). In line with the observed sensitivity in NB cells (Fig. 3*A*), the DP response was largely absent at low concentrations of ceralasertib (50 nM; 19 DP sites; Fig. 4*B*). SET S184 was one of the few dephosphorylated sites at low concentrations. Remarkably, this was also the strongest responding site at high concentrations (Dataset S1).

To identify the protein kinases mediating the DP response, we performed a motif enrichment analysis based on the recently published atlas of substrate specificities for the human serine/threonine kinome (30). This analysis confirmed ATM and DNAPK as the main drivers of the compensatory phosphorylation response. The strongest enrichments for the dephoshorylated motifs were observed for Ribosomal Protein S6 Kinases including RSK4 and P70S6KB; Fig. 4*D* and *SI Appendix*, Fig. S3*A*. While S6K is downstream of mTOR, the predicted downregulation of RSK4 is intriguing, as RSK4 is reported to be constitutively active in most cell types, in contrast to RSK1-3 (31).

We then focused on phosphorylation sites in different PIKK family members (ATM, ATR, DNAPK, or mTOR). Using an unsupervised clustering approach, three obvious clusters were observed (Fig. 4*E*). Cluster 2 contained 65 sites that were mainly dephosphorylated upon elimusertib 50 nM and ceralasertib 1 μM treatment (mean log2FC = −0.37 and −0.38, respectively; $P < 0.001$ for both; *SI Appendix*, Fig. S3*B*) and included ATR T1989, CHK1 S317, and RPTOR S722. This cluster was enriched for sites in proteins active in the ATR pathway (odds ratio = 2.8, $P = 3.3e-03$, Fisher's exact test) as well as the mTOR pathway (odds ratio = 1.8, $P = 0.037$). Cluster 3 was enriched for proteins active in the ATM pathway (odds ratio = 5.26, $P = 3.2e-08$) and contained 63 phosphorylated sites, including ATM S1981, CHK2 S260 and S379, DNAPK S2612, S2624 and S3205 as well as CHK1 S286. Interestingly, while treatment with the low concentration of ceralasertib did not result in any response in the ATM-related cluster 3, a clear dephosphorylation (mean log2FC = − 0.21; $P = 1.1e-10$) was still observed in the ATR-related cluster 2 (Fig. 4*E*).

In conclusion, our phosphoproteomic analysis suggests that ATR inhibition with either 50 nM elimusertib or 1 μM ceralasertib results in a highly similar reduction of ATR and mTOR signaling and a compensatory response that is driven by both ATM and DNAPK. This compensation was absent at low concentrations of ceralasertib.

Use of Elimusertib Results in Long-Term Responses in ALK-Driven NB Mouse Models. We next investigated the efficiency of these ATR inhibitors alone or in combination with lorlatinib in ALK-driven NB mouse models. Alk/MYCN-driven GEMM tumors were treated with either 25 mg/kg elimusertib or ceralasertib twice

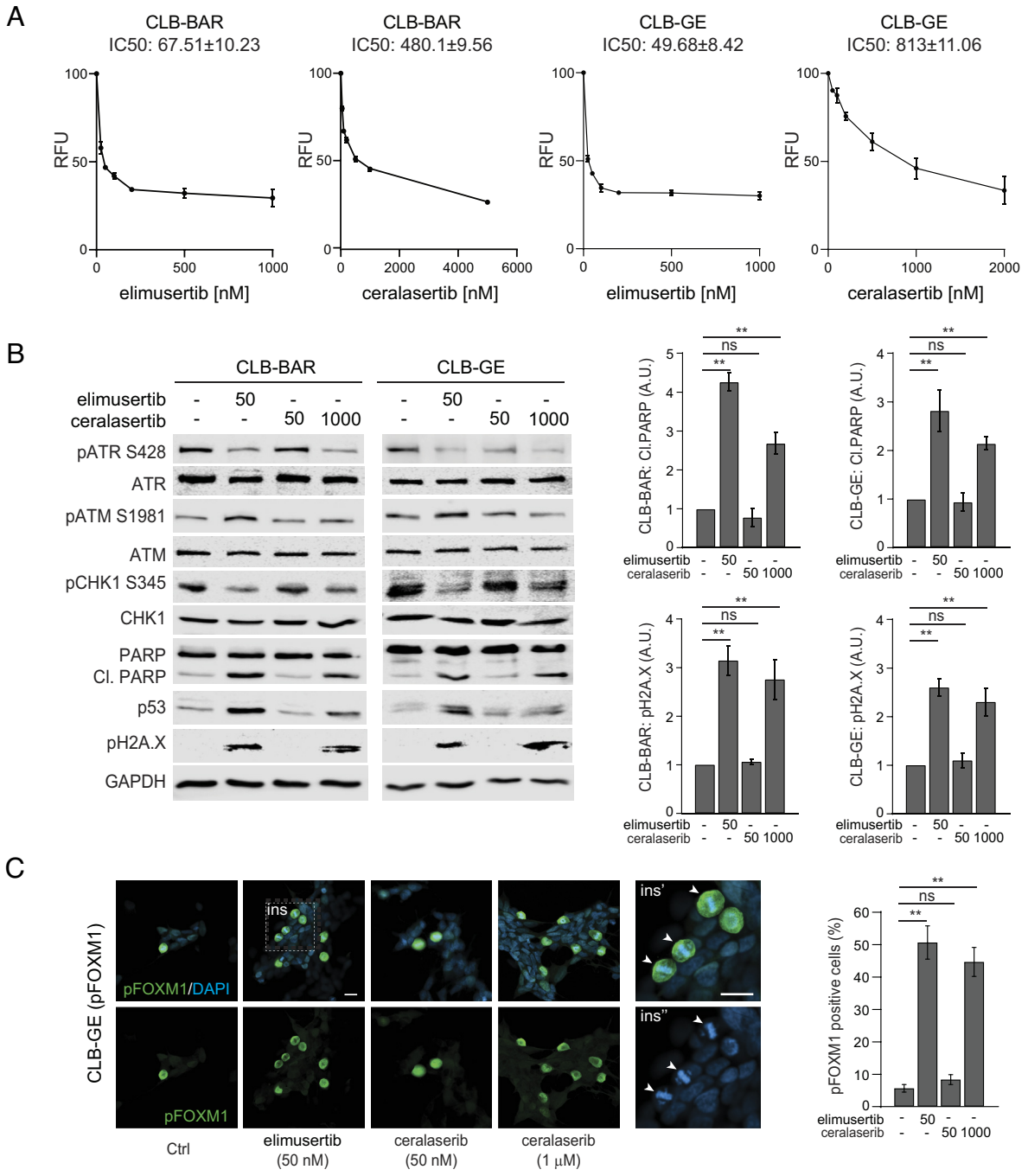

Fig. 3. ALK-positive NB cell lines exhibit differential sensitivity to elimusertib and ceralasertib. (*A*) CLB-BAR and CLB-GE cell viability in response to elimusertib and ceralasertib. Data shown as mean ± SE of fold relative fluorescence units (RFU) relative to untreated cells from three independent experiments. (*B*) ALK-positive CLB-BAR and CLB-GE cells treated for 24 h with elimusertib or ceralasertib as indicated (nM). Lysates were immunoblotted for pATR (S428), ATR, pATM (S1981), ATM, pCHK1 (S345), CHK1, PARP/cl.PARP (quantified at *Right*), p53 and pH2A.X (S139, quantified at *Right*). GAPDH was employed as loading control. (*C*) CLB-GE cells were synchronized by thymidine block for 24 h followed by treatment with elimusertib or ceralasertib as indicated. Cells were stained for pFOXM1 (T600) (green, quantified at right) and DAPI (blue). Panels (ins) indicate close up of cells in metaphase (arrowheads) (scale bar, 20 μm.) Bar graphs indicate the percentage of pFOXM1 T600 (green)-positive cells following elimusertib or ceralasertib treatment. n = 3 biologically independent experiments, unpaired *t* test; ns, not significant; ***P* < 0.01.

daily for two 3-d periods over the 14-d protocol (Fig. 5*A*). For the combinatorial regimen, the initial ATR inhibitor monotreatment (either elimusertib or ceralasertib) was followed by 10 mg/kg lorlatinib twice daily for 11 d, supplemented with the respective ATR inhibitor at days 8 to 10 (Fig. 5*B*). All mice tolerated the treatment regimen with no noticeable side effects. Similar tumor volume decrease was observed in response to both elimusertib and ceralasertib (Fig. 5*C*). In contrast to monotreatment, no tumors were detected at day 14 after treatment in any of the lorlatinib and elimusertib combinatorial treated GEMMs (Fig. 5*C*). However, in lorlatinib and ceralasertib combinatorial treated GEMMs, we observed similar tumor volume decreases to that seen with elimusertib monotreatment (Fig. 5*C*). Taken together, these data indicate that ALK inhibition increases the antitumor efficacy of the ATR inhibitors elimusertib and ceralasertib, in our NB GEMMs.

Given this striking response to the 14-d elimusertib/lorlatinib regimen, we maintained all remaining mice over time without any therapeutic interventions. In addition, mice were subjected

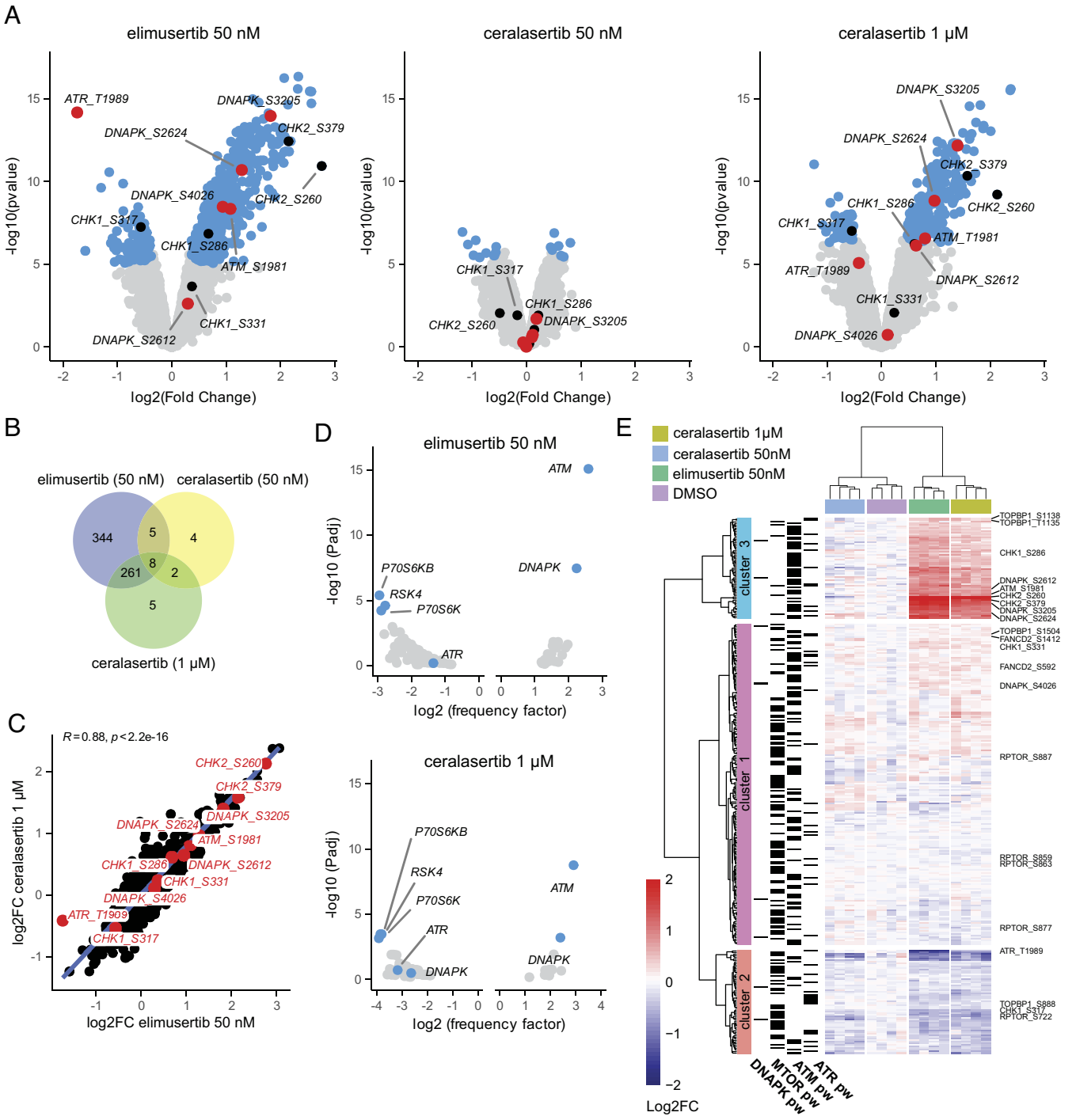

Fig. 4. Comparison of the phosphoproteomic response to elimusertib and ceralasertib treatment of NB cell lines. CLB-BAR cells were synchronized by thymidine block and treated with either DMSO (control), elimusertib (50 nM) and ceralasertib (50 nM or 1 μM) for 6 h. (*A*) Volcano plots showing DP between different treatments (as indicated) and control. DP sites are indicated in blue. ATR, ATM, and DNAPK sites are indicated and labeled in red. CHK1/2 sites are indicated in black. (*B*) Venn diagrams indicating the number of DP sites for each condition. (*C*) Correlation plot between DP log2FC values of different treatments as indicated. Sites in ATR, ATM, DNAPK, and CHK1/2 are indicated and labeled in red. Linear regression line in blue and Pearson correlation coefficient indicated on *Top*. (*D*) Volcano plot showing PK predictions for all hypophosphorylated (negative values) and hyperphosphorylated sites (positive values). ATR, ATM, DNAPK, and strongest predicted PKs are labeled and indicated in blue. (*E*) Heatmap comparing log2FC between different samples as indicated. Hierarchical clustering was performed using the Ward.2 method with dendrograms indicated. Genes active in ATR, ATM, DNAPK, and mTOR pathways (pw) are indicated on the *Left*. See Dataset S1 for detailed results.

to recurrent follow-up by ultrasound, confirming complete tumor regression. All mice treated with ceralasertib alone relapsed within 35 d of treatment cessation. This is similar to the response rate observed by Roeschert and colleagues in a *Th-MYCN* driven NB mouse model (15), employing 25 to 30 mg/kg ceralasertib, where all mice treated died during the 32 d treatment regime. In our hands, the ceralasertib/lorlatinib combination resulted in prolonged survival compared with ceralasertib alone; however, all mice except one relapsed within 76 d of treatment termination (Fig. 5*D*). In comparison, mice treated with elimusertib as a single agent exhibited increased survival when compared with either ceralasertib alone or ceralasertib/

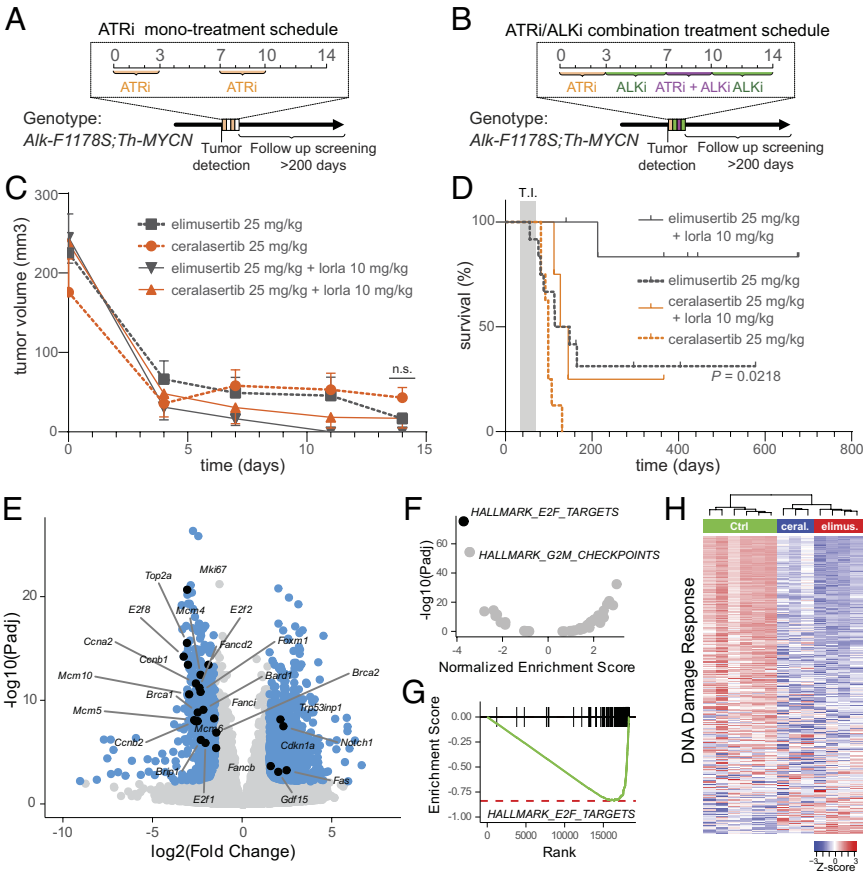

Fig. 5. Elimusertib exhibits a more robust antitumor response in GEMMs compared to ceralasertib. (*A*) Schematic of the monotreatment regimen for Alk/MYCN-driven GEMM tumors. Mice were treated with 25 mg/kg elimusertib or ceralasertib for 3 d. A subsequent 4-d pause from treatment was followed by an additional 3 d of ATRi. (*B*) In the combination regimen, initial monotreatment with ATRi was followed by 10 mg/kg lorlatinib for 11 d, supplemented with ATRi at days 8 to 10, orally. All treatments were given twice daily. (*C*) Tumor volume was measured by ultrasound over 14 d. Data presented as mean ± SEM. (*D*) Survival (from birth) of *Alk-F1178S;Th-MYCN* treated with elimusertib monotreatment (gray dashed, n = 12) or ceralasertib (orange dashed, n = 8) ($P = 0.0218$) compared with elimusertib or ceralasertib and lorlatinib combination treatment (gray and orange solid, respectively, n = 7 and n = 4) ($P = 0.025$). Data for elimusertib and elimusertib/lorlatinib treatment cohorts are shown for comparison. Gray bar indicates tumor incidence (T.I.) range. Data shown as Kaplan–Meier with log-rank (Mantel–Cox) test. (*E*) Volcano plot showing RNA-Seq-based differential gene expression (DE) analysis between untreated control *Alk-F1178S;Th-MYCN* tumors (n = 6) and after 3 d of ceralasertib treatment (n = 3). DE genes are indicated in blue, with genes discussed in the main text indicated in black. (*F* and *G*) Hallmark GSEA showing normalized enrichment scores and corresponding FDR values with running score plot (panel *G*) shown for E2F targets, the most strongly enriched gene set. (*H*) Heatmap comparing z-score normalized gene expression counts between untreated control, ceralasertib treated, and elimusertib treated *Alk-F1178S;Th-MYCN* tumors for 273 different DDR genes as indicated. Genes ranked based on DE (most DE on *Top*). Color key shown at *Bottom Right*. Columns (tumor samples) are hierarchically clustered as illustrated by the dendrogram shown on the *Top*.

lorlatinib in combination, with three out of twelve mice remaining tumor free for more than 230 d after cessation of therapy (Fig. 5*D*). Further, and surprisingly, elimusertib monotreatment is superior to lorlatinib treatment alone in our Alk-driven NB models (14, 19).

Monotreatment with elimusertib had a significantly better survival rate as compared to ceralasertib [log-rank (Mantel–Cox) test, $P = 0.0218$; Fig. 5*D*]. Remarkably, all but one *Alk-F1178S;Th-MYCN* mouse treated with the elimusertib/lorlatinib regimen have remained tumor free (for >290 d from treatment). The single relapsed mouse had a tumor in the lumbar region of the back 137 d after treatment cessation, at age 210 d. However, it is unclear whether this was a recurrence of the original tumor or a newly arising primary tumor. To further characterize the ATR inhibition response, tumors were treated with either elimusertib or ceralasertib for 3 d and sampled for histological and RNA-Seq analysis (14)(Dataset S2). Treated tumors exhibited a reduced tumor volume (*SI Appendix*, Fig. S4*A*), accompanied by reduced staining of the Ki67 proliferation marker and enhanced cleaved caspase 3 activity (CC3) when compared with vehicle controls (*SI Appendix*, Fig. S4*B*). Similar to our previous analysis on elimusertib treated mice (14), RNA-Seq analysis of *Alk-F1178S;Th-MYCN* tumors treated with ceralasertib displayed a downregulation of E2F targets and G2M checkpoint genes (Fig. 5 *E–H*).

Elimusertib Treatment Triggers a Robust Differentiation Response in Tumors. We next tested whether host immune cell involvement may assist in the rapid tumor loss on ATR inhibition. To investigate differences in immune cell infiltration, tumors from mice treated with elimusertib (25 mg/kg), lorlatinib (10 mg/kg), or vehicle twice daily for 3 d were analyzed by FACS with an immune cell panel. No obvious differences in immune cell infiltration of the tumor were observed, with similar relative levels of cells from innate and adaptive lineages (*SI Appendix*, Fig. S5). Subgroup analysis of CD4+ and CD8+ cells also failed to identify any significant changes between the three treatments or expression of the CD69 activation/residential memory marker. CD8 inhibition resulted in a slight decrease in tumor response to the 14-d combination treatment of elimusertib and lorlatinib in *Alk-F1178S;Th-MYCN* mice harboring tumors (Fig. 6*A*). We also

tested the effect of cyclic GMP-AMP synthase/stimulator of IFN genes (cGAS/STING) inhibition, employing the H-151 inhibitor during treatment (32). Notably, treatment with H-151 did not block the rapid tumor regression in mice receiving elimusertib and lorlatinib combination therapy, although it did result in a significant increase (P = 0.0129) in relapse after treatment in comparison with elimusertib and lorlatinib (Fig. 6 *B* and *C*). Thus, while immune cell responses appear to be important for the prolonged response observed in tumor bearing *Alk-F1178S;Th-MYCN* mice in response to combined ATR inhibition, neither CD8+ T cells nor the cGAS/STING response seem to be required for the rapid tumor response observed on ATR inhibition.

Having been unable to identify a role for either the CD8+ T cells or the cGAS/STING response in the rapid tumor regression response, we conducted an in-depth histopathological examination of ALKi/ATRi treated tumors that revealed tumor areas exhibiting characteristics of differentiation resembling neuronal or Schwann cell tissue (Fig. 6*D*), observed in tumors treated with ATR inhibitors. Prompted by these findings, we searched for cellular differentiation signals in our elimusertib treated tumor derived RNA-seq data, employing GSEA analysis using cell type signature gene sets derived from PanglaoDB and MSigDB. Remarkably, the strongest enrichments were found for neuronal gene sets, and also, Schwann cells (or their precursors) were significantly enriched in both datasets (Fig. 6 *E* and *F*). Neuronal gene set enrichments were confirmed by focusing the analysis on gene sets derived from previous chemical and genetic perturbation experiments in mice, which also indicated strong depletion of genes up-regulated in neuroendocrine lung carcinoma (*SI Appendix*, Fig. S6).

Taken together, these data suggest that ATR inhibition triggers a differentiation response in mouse tumors. In agreement, a number of markers in the Schwann cell differentiation pathway were confirmed by immunohistochemistry. These included Mag and Mpz, which were expressed in *Alk-F1178S;Th-MYCN* tumors treated with elimusertib and lorlatinib (Fig. 6*G*). We also noted increased Sox10 positivity on treatment with elimusertib and lorlatinib; however, untreated control tumors also contained Sox10 positive cells in some areas. To test further the hypothesis that ATR inhibition triggers differentiation, we treated NB cells with low doses of ATR inhibitor in the presence or absence of retinoic acid (RA) and asked whether ATR inhibition was able to potentiate RA-induced differentiation. While RA treatment induced neuronal differentiation in 36% of SK-N-BE(2) cells, addition of low dose elimusertib further induced neuronal differentiation to 63% in a dose-dependent manner (Fig. 6*H* and *SI Appendix*, Fig. S7*A*). Neurite length and branch points were significantly increased by low dose elimusertib in the presence of RA, compared to RA treated controls (Fig. 6*H*). Consistent with the neuronal differentiation phenotype, expression of established neuronal lineage differentiation markers, such as RET, DLG2, MAP2A, and NSE, was further up-regulated in by elimusertib in the presence of RA (*SI Appendix*, Fig. S7*B*).

Tumors Treated with Elimusertib Exhibit Differential DNA Methylation. We next considered the possibility that ATRi-induced differentiation is due to an effect of the DDR on genome methylation. Epigenetic regulation, including DNA methylation, plays an important role in NB (33), prompting us to examine changes in DNA methylation in *Alk-F1178S;Th-MYCN* tumors treated with elimusertib for 72 h. Strikingly, immunohistochemical staining of ATRi-treated tumors for 5-methylcytosine (5-mC) revealed a considerable increase in DNA methylation, together with a Schwann cell–like phenotype (Fig. 6*I*). Whole-genome bisulfite sequencing (WGBS) identified a global augmentation in differentially methylated regions (DMRs) in ATR-inhibited tumors, with elevated numbers of hypermethylated regions observed on each chromosome, consistent with increased levels of 5-mC (Fig. 6*J*, *SI Appendix*, Fig. S8 *A*–*C*, and Dataset S3). Specifically, an increase in methylated CpG islands and shores throughout the genome was observed, accompanied by intensified methylation within gene bodies, encompassing exons, introns, and untranslated regions in ATRi-treated tumors (Fig. 6*K* and *SI Appendix*, Fig. S8 *D* and *E*). We also identified distinct genomic regions that exhibited higher levels of methylation, surpassing the DMR threshold of >0.5 (Fig. 6*L*). To gain insights into cellular processes influenced by ATR inhibition, we analyzed highly hypermethylated gene bodies (DMR < 0.5) identifying differences in DMR levels between elimusertib and vehicle treated tumors (ΔDMR < 0.2) (*SI Appendix*, Fig. S8*F*). Several among the 10 most significant clusters encompassed methylated gene bodies associated with developmental processes. Among interesting loci hypermethylated in response to ATRi, we noted components of the TGF-beta signaling and Ephrin pathways (e.g., *Tgfb1*, *Tgfbr3*, *Ephb3*, and *Ephb4*), interesting as cross-talk between TGF-β and Ephrin pathways interferes with Schwann cell differentiation to drive peripheral nerve regeneration (34). Additionally, we detected hypermethylation in *Fgfr2*, which is intriguing as inhibiting *Fgfr2* has shown promise in sensitizing *MYCN*-amplified NB to CHK1 inhibitors (35). Hypomethylated regions were less frequent but still present following ATRi treatment (*SI Appendix*, Fig. S8*F*), and cluster analysis revealed five significant clusters involving cell adhesion. Collectively, our findings provide compelling evidence that ATR inhibition induces widespread hypermethylation in treated tumors. Further investigations are warranted to elucidate the role of gene methylation in differentiation and response to ATR inhibitors in NB.

Discussion

Management of high-risk NB presents a serious clinical challenge. The identification of ALK mutations in NB, together with the synergistic effect of ALK with MYCN in driving aggressive and penetrant NB in both preclinical models and from clinical data, has raised hopes that ALK inhibition will be therapeutically beneficial in NB patients (4, 36–39). As a result, ALK mutation–positive NB patients are treated with ALK inhibitors, which typically elicit a strong response, and there have been reports of long-term responses (8, 40–42). However, patients treated with ALK TKIs also relapse with a complex landscape of potential resistance mutations (8, 43, 44). Therefore, discovering therapeutic approaches that enhance the efficacy of ALK TKI therapy is a significant objective for the NB research community.

In recent years, ALK TKI combinatorial options with clinically therapeutic potential have been identified (14, 26, 45–47). ATR is one such combination target, with exceptional outcomes in preclinical ALK-driven models (14). ATR inhibitors have been explored in NB, either as monotherapy or in combination with PARP or Aurora-A inhibitors to block NB tumor and cell growth (15, 16, 48). ATR inhibitors in patient clinical trials include M6620 and M4344 (Merck), ceralasertib (Astra Zeneca) (49–51) as well as elimusertib (Bayer) (52, 53) and camonsertib (Repare Therapeutics/Roche) (54) that are currently at various phases (www.clinicaltrials.gov).

The initial combination of ATR and ALK inhibition employed a simple 14-d protocol that resulted in complete tumor resolution in ALK/MYCN-driven NB GEMMs (14). This can be compared to monotreatment with lorlatinib alone, which impairs tumor growth, but is unable to resolve tumors in ALK-driven NB

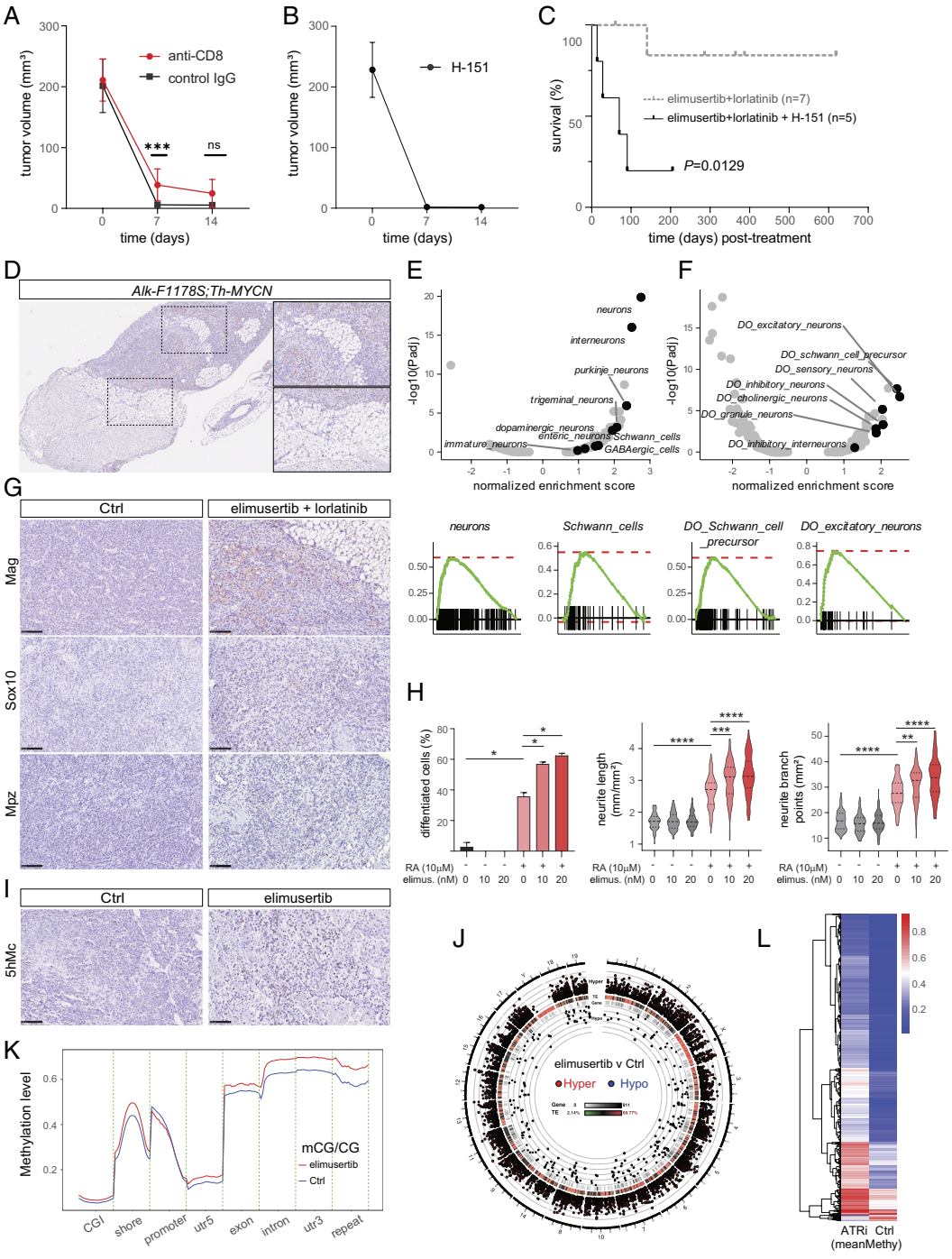

Fig. 6. Investigation of immune cell dependency, differentiation, and methylation upon ATRi treatment. (*A*) Tumor volume in *Alk-F1178S;Th-MYCN* mice harboring tumors treated with combination elimusertib and lorlatinib concurrent with injections of either anti-mouse CD8α [n = 10 (day 0), n = 10 (day 7), and n = 9 (day 14)] or IgG2b isotype control [n = 5 (day 0), n = 5 (day 7), and n = 4 (day 14)]. Tumor volumes of anti-mouse CD8α and IgG2b isotype treated controls at day 7 ($P = 0.0007$) and day 14 ($P = 0.0755$) was compared by two-tailed Mann–Whitney test. (*B*) *Alk-F1178S;Th-MYCN* mice harboring tumors treated with H-151 (n = 5) in addition to the 14-d combination treatment regime (elimusertib+lorlatinib). Tumor volume data are presented as mean ± SD. (*C*) Kaplan–Meier survival curve (posttreatment) of *Alk-F1178S;Th-MYCN* mice harboring tumors treated with H-151 (n = 5) in addition to the 14-d combination treatment regime (elimusertib+lorlatinib). The gray dashed line shows survival curve for elimusertib and lorlatinib alone (Fig. 5*D*) for comparison. Kaplan–Meier survival curve with log-rank (Mantel–Cox) test, $P = 0.0129$. (*D*) Representative elimusertib+lorlatinib treated *Alk-F1178S;Th-MYCN* tumor, showing distinct histological features within the same tumor; inserts are magnifications of dashed squares. (*E* and *F*) Volcano plots showing GSEA results using cell type signature genes from PanglaoDB (*E*) and MSigDB (*F*). Enrichment was performed using DGE between NB tumors from *Alk-F1178S;Th-MYCN* mice in untreated control conditions (n = 6) and after 3 d of elimusertib treatment (n = 3). Neuronal and Schwann cell–related gene sets are indicated. Lower plots show running score plots for the most enriched neuronal and Schwann cell–related gene sets. (*G*) Sections from control and elimusertib+lorlatinib treated tumors were stained for Mag, Sox10, and Mpz by immunohistochemistry. Treated tumors exhibited Mag- and Mpz-positive regions with enlarged cells resembling neuronal or Schwann cells. Control tumors were negative. Sox10-positive nuclei were present in both control and treated tumors. (*H*) Bar graphs indicate percentage of differentiated SK-N-BE(2) cells, neurite length (mm/mm^2), and neurite branch points (mm^2) following RA or/and elimusertib treatment for 24 h. n = 3 biologically independent experiments. Unpaired two-tailed *t* test (*$P < 0.05$, **$P < 0.01$, ***$P < 0.001$, and ****$P < 0.0001$). (*I*) Sections from control and elimusertib treated tumors were stained for 5-hydroxymethylcytosine (5-hmC) by immunohistochemistry. Treated tumors exhibited 5-hmC-positive regions with enlarged cells resembling neuronal or Schwann cells. (*J*) Circos plot showing hypo- and hypermethylated regions within the mouse genome between vehicle and elimusertib treated *Alk-F1178S;Th-MYCN* tumors. (*K*) Diagram showing methylation levels within functional genomic regions. (*L*) Heatmap of DMR between vehicle and elimusertib treatment. Vehicle treatment n = 3, elimusertib treatment n = 3 in (*K* and *L*). DMRs were sorted by areaStat including hypomethylated (areaStat < 0) and hypermethylated (areaStat > 0) DMRs.

GEMMs (19). Upon cessation of ALK inhibitor treatment, tumor growth resumes aggressively. Remarkably, in this study, we show that ATRi monotreatment is sufficient to resolve ALK-driven tumors. Surprisingly, ATRi monotreatment displays better efficacy than lorlatinib in an ALK/MYCN-driven mouse model, while combined ATR/ALK inhibition resulted in a significantly increased long-term survival benefit. At the molecular level, we have identified the impact of ALK signaling on the DDR via phosphorylation of both ATR and CHK1. The ALK-responsive CHK1-S280 phosphorylation site, rather than the ATR site (CHK1-S345), has previously been reported to be downstream of both Akt and p90RSK (22, 55). Taken together, our findings suggest that ALK signaling in NB supports the robustness of the DDR (14, 20). Previous RNA interference (RNAi) screening of kinases identified CHK1 as a therapeutic target in NB cell lines, also showing that high-risk NB exhibits increased CHK1 expression and activation (56). Our identification of ALK-regulated phosphorylation of CHK1-S280 suggests that combination of ALK and ATR inhibition results in a more effective impairment of CHK1 function.

In this study, we compared two ATR inhibitors, elimusertib and ceralasertib, and show that both drugs are effective in resolving ALK-driven tumors in our GEMMs. However, tumor-bearing animals treated with ceralasertib relapse significantly faster than those treated with elimusertib. Our phosphoproteomics analyses also suggest that elimusertib is more potent in NB cells, with 1 μM ceralasertib resulting in similar, but not identical, phosphoproteomic profiles to 50 nM elimusertib. Both drugs led to compensation of ATR inhibition by upregulation of ATM and DNAPK activity. We have previously noted the compensatory activation of ATM (14). In the present study we have employed the recently reported atlas of substrate specificities for the human serine/threonine kinome (30), which identified increased DNAPK activity in response to ATR inhibitor treatment. This is further supported by our observation of increased phosphorylation on DNAPK-S3205, which has been reported as both a DNAPK autophosphorylation site (57), and a target of ATM (58).

The rapid reduction in tumor size led us to investigate a role for the immune system in this process. However, although inhibition of T cells with anti-CD8 antibodies had some effect, it failed to block tumor shrinkage in response to ATR inhibition. Likely, activation of the T cell compartment plays a role in the long-lasting response observed in these mice, an aspect that will be important to investigate in future studies. Interestingly, a recent study has reported that ATRi treatment cessation can potentiate T cell responses, suggesting that our 14-d schedule may be beneficial (59). Given that targeting of the DDR leads to activation of the cGAS-STING pathway, we also investigated whether blocking this pathway with the H-151 inhibitor, that blocks activation-induced palmitoylation of STING (32), would affect tumor shrinkage in response to ATR inhibition. Again, while we show that activation of cGAS-STING appears to be important for the long-term prevention of relapse, we could not obtain any strong evidence that this pathway plays an important role in the rapid tumor response.

A key finding in this work is the observed differentiation of tumors in response to ATR inhibition. Induction of differentiation in NB is considered a therapeutically exploitable option, with treatments such as RA employed in the clinic to promote differentiation (60–62). In the current era of high-tech data analyses, it is easy to overlook simple methodology. Routine histological analysis of tumors treated with ATR inhibitors revealed large regions of tumor that resembled adipose or neural tissue. RNA-seq analyses of treated tumors identified a strong enrichment of neuronal and Schwann cell gene sets. Interestingly, earlier work has shown that deletion of *Atr* in adult mice leads to depletion of stem and progenitor cells (63), that has been suggested to arise due to aberrant, ectopic differentiation. This hypothesis is supported by a recent report in the fruitfly, which identified a critical role for *Drosophila* ATR (*mei-41*) in preventing neuroblast differentiation in response to irradiation stress (64). Interestingly, inhibition of the ATR and ATM DDR kinases has been linked with differentiation in acute myeloid leukemia cells carrying MLL fusion proteins, where treatment with ATR inhibitors led to terminal differentiation and loss of leukemic blasts (65, 66). We show here that low-dose elimusertib synergizes with RA, suggesting that ATR inhibition may increase the potential of differentiation therapy in NB and highlights the need to elucidate the mechanisms underlying the ATR inhibition–induced differentiation response in our NB tumor models. Ultimately, ATR inhibition may promote multiple important tumor effects by promoting NB differentiation as well impairing the DDR leading to mitotic catastrophe. The effect of ATR inhibition on the tumor epigenome we observed in vivo is supported by many studies linking the DDR and genome methylation. While detailed investigation is beyond the scope of this study, we note differential methylation of many loci involved in neuronal differentiation that will be interesting to examine in future work.

Our findings show that this ALKi/ATRi 14-d combination treatment is highly effective in ALK-driven GEMM models of NB. However, several questions remain. For example, is this treatment useful for non-ALK-driven NB? *Th-MYCN* tumors exhibit high levels of replication stress, which suggests they would be sensitive to ATR inhibition, and indeed treatment with ceralasertib has already been reported in preclinical models (15). To our knowledge, there are few reported clinical NB cases in which ATR inhibitors have been employed (67), and the question of which patients may benefit most is important to consider. High-risk NB patients exhibiting *MYCN*-amplification, *ALK*-activating mutations and overexpression/amplification, combined *MYCN*/*ALK* perturbations and 2p-gain, are all NB categories that potentially exhibit high levels of oncogene-induced replicative stress and may be sensitive to ATR inhibition. An additional high-risk NB category of interest are the 11q-deletion group, where many genes involved in the DDR, such as *ATM*, *CHEK1*, *H2AFX,* and *MRE11*, are lost (6). In future work, it will be interesting to focus on the potential of ATR inhibition in these different genetic categories. It will also be important to consider means of identifying NB cases that may respond to ATR inhibition. In this respect, a recent study identified nuclear pCHK1 as a potential biomarker of ATR sensitivity to ATR inhibition (68).

NB tumors harboring activating RAS mutations such as *NRASQ61** or *KRASQ61** (5, 69) would also be expected to exhibit high levels of replication stress, and 50 nM elimusertib is highly effective in preventing growth of SKNAS NB cells (14), making it of interest to test whether this ATRi/ALKi combination, or perhaps an ATRi/MEKi combination, would be effective in a *RAS* mutant NB setting. This is of particular interest considering recent findings that have identified potential *RAS* mutant resistance mutations in lorlatinib treated NB patients (8).

Ultimately, this work identifies ALKi/ATRi combination therapy as an effective treatment in ALK-driven NB GEMMs. We further show that ALK signaling primes the DDR through phosphorylation of ATR and CHK1, providing an underlying molecular mechanism. The strong neuronal and Schwann cell signatures observed in tumors treated with ATR inhibitors, together with increased DNA methylation levels, suggest that ATR inhibition exerts a robust differentiation response that underlies tumor

regression. Taken together, these results strongly motivate the continued exploration of ATR/ALK inhibition as a potentially therapeutically effective approach in NB.

Methods

CLB-BAR, CLB-GE, CLB-GAR, SK-N-BE(2), IMR32, and NB1 NB cell lines were used to study the effects of ATR, ALK, or CHK1 inhibitors, as well as etoposide or RA treatment, in the presence or absence of ALKAL2 stimulation. Protein expression and phosphorylation level were investigated by immunoblotting on whole-cell lysates and subcellular fractions. Effects on cell growth and neurite outgrowth were monitored by IncuCyte Live cell system. In addition, RNA sequencing and phosphoproteomic analyses were performed. *Alk-F1178S*$^{KI/0}$;*Th-MYCN*$^{Tg/0}$ murine tumors were treated with ATR inhibitor and/or lorlatinib, administered orally twice per day for 14 d, with or without immune system modulation. Tumor volume and tumor free survival was monitored for up to 700 d. Additionally, short-term tumor treatment with ATR inhibitors was performed for immunohistochemistry, transcriptomics, WGBS, and immune cell sorting. Statistical, data, and gene set enrichment analyses were performed using GraphPad Prism software or the R statistical package.

Data, Materials, and Software Availability. The mass spectrometry proteomics data have been deposited to the Proteome Xchange Consortium (70) via the PRIDE (71) partner repository with the dataset identifier PXD041824 and the MassIVE partner repository (https://massive.ucsd.edu/ProteoSAFe/static/massive.jsp) with the dataset identifier MSV000092789. RNA-seq data are available in ArrayExpress (https://www.ebi.ac.uk/arrayexpress/, accession number: E-MTAB-12961). All other data required to evaluate the conclusions in the paper are provided in *SI Appendix*. Source code used for the RNA-Seq and downstream proteomics analysis is available at GitHub https://github.com/CCGGlab/ATR_AZD.

ACKNOWLEDGMENTS. We thank Palmer/Hallberg lab members for critical feedback. For proteomics and phosphoproteomics analysis, we thank Dr. E. Berger and Dr. C. Sihlbom at the Proteomics Core Facility at Sahlgrenska Academy, University of Gothenburg. This work has been supported by the Swedish Cancer Society (RHP:CAN21/01549; BH:CAN21/1525), the Swedish Children's Cancer Foundation (RHP:2019-0078; BH:2021-0027), the Swedish Research Council (RHP:2019-03914; BH:2021-1192), the Swedish Foundation for Strategic Research (RB13-0204), the Knut and Alice Wallenberg Foundation (KAW:2015.0144), the Assar Gabrielsson's Foundation (MBo:FB22-89), the Wenner-Gren Foundation (RHP:2021-0004), the Swiss National Science Foundation (MNH:310030/192493), Ghent University Special Research Fund (JVdE:BOF.STG.2019.0073.01), and Research Foundation Flanders (JVdE V424522N).

Author affiliations: [a]Department of Medical Biochemistry and Cell Biology, Institute of Biomedicine, Sahlgrenska Academy, University of Gothenburg, Gothenburg SE-405 30, Sweden; [b]Proteomics Core Facility, Biozentrum, Basel University, Basel 4056, Switzerland; [c]Department of Human Structure and Repair, Anatomy and Embryology Unit, Ghent University, Ghent 9000, Belgium; [d]Department of Microbiology and Immunology, Institute of Biomedicine, Sahlgrenska Academy, University of Gothenburg, Gothenburg SE-405 30, Sweden; [e]Department of Clinical Immunology and Transfusion Medicine, Sahlgrenska University Hospital, Gothenburg SE-405 30, Sweden; and [f]Biozentrum, University of Basel, Basel 4056, Switzerland

Author contributions: M. Borenäs, G.U., D.E.L., W.-Y.L., J.G., B.H., J.V.d.E. and R.H.P. designed research; M. Borenäs, G.U., D.E.L., W.-Y.L., J.G., J.J., E.J., A. Schmidt, Y.K., A.A., A. Strömberg, M. Bemark, J.V.d.E. and R.H.P. performed research; M.N.H., J.V.d.E., B.H. and R.H.P. contributed new reagents/analytic tools; M. Borenäs, G.U., D.E.L., W.-Y.L., J.G., J.J., E.J., A. Schmidt, J.L.G., M. Bemark, J.V.d.E., B.H., and R.H.P. analyzed data; and M. Borenäs, G.U., D.E.L., W.-Y.L., J.G., J.J., E.J., A. Schmidt, J.L.G., M. Bemark, M.N.H., J.V.d.E., B.H., and R.H.P. wrote the paper.

1. K. K. Matthay *et al.*, Neuroblastoma. *Nat. Rev. Dis. Primers* **2**, 16078 (2016).
2. R. Ladenstein *et al.*, Busulfan and melphalan versus carboplatin, etoposide, and melphalan as high-dose chemotherapy for high-risk neuroblastoma (HR-NBL1/SIOPEN): An international, randomised, multi-arm, open-label, phase 3 trial. *Lancet Oncol.* **18**, 500–514 (2017).
3. L. Amoroso *et al.*, Topotecan-vincristine-doxorubicin in stage 4 high-risk neuroblastoma patients failing to achieve a complete metastatic response to rapid COJEC: A SIOPEN study. *Cancer Res. Treat.* **50**, 148–155 (2018).
4. S. De Brouwer *et al.*, Meta-analysis of neuroblastomas reveals a skewed ALK mutation spectrum in tumors with MYCN amplification. *Clin. Cancer Res.* **16**, 4353–4362 (2010).
5. T. J. Pugh *et al.*, The genetic landscape of high-risk neuroblastoma. *Nat. Genet.* **45**, 279–284 (2013).
6. J. Guan, B. Hallberg, R. H. Palmer, Chromosome imbalances in neuroblastoma-recent molecular insight into chromosome 1p-deletion, 2p-gain, and 11q-deletion identifies new friends and foes for the future. *Cancers (Basel)* **13**, 5897 (2021).
7. B. Qiu, K. K. Matthay, Advancing therapy for neuroblastoma. *Nat. Rev. Clin. Oncol.* **19**, 515–533 (2022).
8. K. C. Goldsmith *et al.*, Lorlatinib with or without chemotherapy in ALK-driven refractory/relapsed neuroblastoma: Phase 1 trial results. *Nat. Med.* **29**, 1092–1102 (2023), 10.1038/s41591-023-02297-5.
9. R. C. Seeger *et al.*, Association of multiple copies of the N-myc oncogene with rapid progression of neuroblastomas. *N. Engl. J. Med.* **313**, 1111–1116 (1985).
10. M. L. Schmidt *et al.*, Biologic factors determine prognosis in infants with stage IV neuroblastoma: A prospective Children's Cancer Group study. *J. Clin. Oncol.* **18**, 1260–1268 (2000).
11. F. J. Groelly, M. Fawkes, R. A. Dagg, A. N. Blackford, M. Tarsounas, Targeting DNA damage response pathways in cancer. *Nat. Rev. Cancer* **23**, 78–94 (2023).
12. J. C. Saldivar, D. Cortez, K. A. Cimprich, The essential kinase ATR: Ensuring faithful duplication of a challenging genome. *Nat. Rev. Mol. Cell Biol.* **18**, 622–636 (2017).
13. L. I. Toledo *et al.*, ATR prohibits replication catastrophe by preventing global exhaustion of RPA. *Cell* **155**, 1088–1103 (2013).
14. J. Szydzik *et al.*, ATR inhibition enables complete tumour regression in ALK-driven NB mouse models. *Nat. Commun.* **12**, 6813 (2021).
15. I. Roeschert *et al.*, Combined inhibition of Aurora-A and ATR kinase results in regression of MYCN-amplified neuroblastoma. *Nat. Cancer* **2**, 312–326 (2021).
16. H. E. D. Southgate, L. Chen, D. A. Tweddle, N. J. Curtin, ATR inhibition potentiates PARP inhibitor cytotoxicity in high risk neuroblastoma cell lines by multiple mechanisms. *Cancers (Basel)* **12**, 1095 (2020).
17. S. L. George *et al.*, Novel therapeutic strategies targeting telomere maintenance mechanisms in high-risk neuroblastoma. *J. Exp. Clin. Cancer Res.* **39**, 78 (2020).
18. J. Guan *et al.*, The ALK inhibitor PF-06463922 is effective as a single agent in neuroblastoma driven by expression of ALK and MYCN. *Dis. Model Mech.* **9**, 941–952 (2016).
19. M. Borenas *et al.*, ALK ligand ALKAL2 potentiates MYCN-driven neuroblastoma in the absence of ALK mutation. *EMBO J.* **40**, e105784 (2021).
20. J. Van den Eynden *et al.*, Phosphoproteome and gene expression profiling of ALK inhibition in neuroblastoma cell lines reveals conserved oncogenic pathways. *Sci. Signal.* **11**, eaar5680 (2018).
21. V. Leung-Pineda, C. E. Ryan, H. Piwnica-Worms, Phosphorylation of Chk1 by ATR is antagonized by a Chk1-regulated protein phosphatase 2A circuit. *Mol. Cell Biol.* **26**, 7529–7538 (2006).
22. P. Li *et al.*, P90 RSK arranges Chk1 in the nucleus for monitoring of genomic integrity during cell proliferation. *Mol. Biol. Cell* **23**, 1582–1592 (2012).
23. T. A. Knijnenburg *et al.*, Genomic and molecular landscape of DNA damage repair deficiency across The Cancer Genome Atlas. *Cell Rep.* **23**, 239–254.e6 (2018).
24. J. T. Siaw *et al.*, 11q deletion or ALK activity curbs DLG2 expression to maintain an undifferentiated state in neuroblastoma. *Cell Rep.* **32**, 108171 (2020).
25. J. T. Siaw *et al.*, Loss of RET promotes mesenchymal identity in neuroblastoma cells. *Cancers (Basel)* **13**, 1909 (2021).
26. E. R. Tucker *et al.*, Combination therapies targeting ALK-aberrant neuroblastoma in preclinical models. *Clin. Cancer Res.* **29**, 1317–1331 (2023).
27. G. Umapathy *et al.*, MEK inhibitor trametinib does not prevent the growth of anaplastic lymphoma kinase (ALK)-addicted neuroblastomas. *Sci. Signal.* **10**, eaam7550 (2017).
28. J. C. Saldivar *et al.*, An intrinsic S/G2 checkpoint enforced by ATR. *Science* **361**, 806–810 (2018).
29. S. Schlam-Babayov *et al.*, Phosphoproteomics reveals novel modes of function and inter-relationships among PIKKs in response to genotoxic stress. *EMBO J.* **40**, e104400 (2021).
30. J. L. Johnson *et al.*, An atlas of substrate specificities for the human serine/threonine kinome. *Nature* **613**, 759–766 (2023).
31. B. A. Dummler *et al.*, Functional characterization of human RSK4, a new 90-kDa ribosomal S6 kinase, reveals constitutive activation in most cell types. *J. Biol. Chem.* **280**, 13304–13314 (2005).
32. S. M. Haag *et al.*, Targeting STING with covalent small-molecule inhibitors. *Nature* **559**, 269–273 (2018).
33. I. S. Fetahu, S. Taschner-Mandl, Neuroblastoma and the epigenome. *Cancer Metastasis Rev.* **40**, 173–189 (2021).
34. M. P. Clements *et al.*, The wound microenvironment reprograms Schwann cells to invasive mesenchymal-like cells to drive peripheral nerve regeneration. *Neuron* **96**, 98–114.e7 (2017).
35. K. Ando *et al.*, FGFR2 loss sensitizes MYCN-amplified neuroblastoma CHP134 cells to CHK1 inhibitor-induced apoptosis. *Cancer Sci.* **113**, 587–596 (2022).
36. T. Berry *et al.*, The ALK(F1174L) mutation potentiates the oncogenic activity of MYCN in neuroblastoma. *Cancer Cell* **22**, 117–130 (2012).
37. S. Zhu *et al.*, Activated ALK collaborates with MYCN in neuroblastoma pathogenesis. *Cancer Cell* **21**, 362–373 (2012).
38. N. Javanmardi *et al.*, Analysis of ALK, MYCN and the ALK ligand ALKAL2 (FAM150B/AUGalpha) in neuroblastoma patient samples with chromosome arm 2p rearrangements. *Genes Chromosomes Cancer* **59**, 50–57 (2019), 10.1002/gcc.22790.
39. G. Umapathy, P. Mendoza-Garcia, B. Hallberg, R. H. Palmer, Targeting anaplastic lymphoma kinase in neuroblastoma. *APMIS* **127**, 288–302 (2019), 10.1111/apm.12940.
40. J. Guan *et al.*, Clinical response of the novel activating ALK-I1171T mutation in neuroblastoma to the ALK inhibitor ceritinib. *Cold Spring Harb. Mol. Case Stud.* **4**, a002550 (2018).
41. D. Treis *et al.*, Sustained response to entrectinib in an infant with a germline ALKAL2 variant and refractory metastatic neuroblastoma with chromosomal 2p gain and anaplastic lymphoma kinase and tropomyosin receptor kinase activation. *JCO Precis. Oncol.* **6**, e2100271 (2022).
42. M. Fischer *et al.*, Ceritinib in paediatric patients with anaplastic lymphoma kinase-positive malignancies: An open-label, multicentre, phase 1, dose-escalation and dose-expansion study. *Lancet Oncol.* **22**, 1764–1776 (2021).
43. G. Schleiermacher *et al.*, Emergence of new ALK mutations at relapse of neuroblastoma. *J. Clin. Oncol.* **32**, 2727–2734 (2014).

44. K. R. Bosse *et al.*, Serial profiling of circulating tumor DNA identifies dynamic evolution of clinically actionable genomic alterations in high-risk neuroblastoma. *Cancer Discov.* **12**, 2800–2819 (2022).
45. E. Uckun *et al.*, BioID-screening identifies PEAK1 and SHP2 as components of the ALK proximitome in neuroblastoma cells. *J. Mol. Biol.* **433**, 167158 (2021).
46. N. F. Moore *et al.*, Molecular rationale for the use of PI3K/AKT/mTOR pathway inhibitors in combination with crizotinib in ALK-mutated neuroblastoma. *Oncotarget* **5**, 8737–8749 (2014).
47. A. C. Wood *et al.*, Dual ALK and CDK4/6 inhibition demonstrates synergy against neuroblastoma. *Clin. Cancer Res.* **23**, 2856–2868 (2017).
48. D. King *et al.*, Increased replication stress determines ATR inhibitor sensitivity in neuroblastoma cells. *Cancers (Basel)* **13**, 6215 (2021).
49. R. Kim *et al.*, Phase II study of ceralasertib (AZD6738) in combination with durvalumab in patients with advanced/metastatic melanoma who have failed prior anti-PD-1 therapy. *Ann. Oncol.* **33**, 193–203 (2022).
50. M. Kwon *et al.*, Phase II study of ceralasertib (AZD6738) in combination with durvalumab in patients with advanced gastric cancer. *J. Immunother. Cancer* **10**, e005041 (2022).
51. E. C. Patin *et al.*, Harnessing radiotherapy-induced NK-cell activity by combining DNA damage-response inhibition and immune checkpoint blockade. *J. Immunother. Cancer* **10**, e004306 (2022).
52. A. M. Wengner *et al.*, The novel ATR inhibitor BAY 1895344 is efficacious as monotherapy and combined with DNA damage–inducing or repair-compromising therapies in preclinical cancer models. *Mol. Cancer Ther.* **19**, 26–38 (2020).
53. T. A. Yap *et al.*, First-in-human trial of the oral ataxia telangiectasia and RAD3-related (ATR) inhibitor BAY 1895344 in patients with advanced solid tumors. *Cancer Discov.* **11**, 80–91 (2021).
54. A. Roulston *et al.*, RP-3500: A novel, potent, and selective ATR inhibitor that is effective in preclinical models as a monotherapy and in combination with PARP inhibitors. *Mol. Cancer Ther.* **21**, 245–256 (2022).
55. E. Shtivelman, J. Sussman, D. Stokoe, A role for PI 3-kinase and PKB activity in the G2/M phase of the cell cycle. *Curr. Biol.* **12**, 919–924 (2002).
56. K. A. Cole *et al.*, RNAi screen of the protein kinome identifies checkpoint kinase 1 (CHK1) as a therapeutic target in neuroblastoma. *Proc. Natl. Acad. Sci. U.S.A.* **108**, 3336–3341 (2011).
57. P. Douglas *et al.*, Identification of in vitro and in vivo phosphorylation sites in the catalytic subunit of the DNA-dependent protein kinase. *Biochem. J.* **368**, 243–251 (2002).
58. A. Bensimon *et al.*, ATM-dependent and -independent dynamics of the nuclear phosphoproteome after DNA damage. *Sci. Signal.* **3**, rs3 (2010).
59. F. P. Vendetti *et al.*, The schedule of ATR inhibitor AZD6738 can potentiate or abolish antitumor immune responses to radiotherapy. *JCI Insight* **8**, e165615 (2023).
60. M. Zeineldin, A. G. Patel, M. A. Dyer, Neuroblastoma: When differentiation goes awry. *Neuron* **110**, 2916–2928 (2022).
61. H. de The, Differentiation therapy revisited. *Nat. Rev. Cancer* **18**, 117–127 (2018).
62. N. Bayeva, E. Coll, O. Piskareva, Differentiating neuroblastoma: A systematic review of the retinoic acid, its derivatives, and synergistic interactions. *J. Pers. Med.* **11**, 211 (2021).
63. Y. Ruzankina *et al.*, Deletion of the developmentally essential gene ATR in adult mice leads to age-related phenotypes and stem cell loss. *Cell Stem Cell* **1**, 113–126 (2007).
64. X. Xu *et al.*, HR repair pathway plays a crucial role in maintaining neural stem cell fate under irradiation stress. *Life Sci. Alliance* **6**, e202201802 (2023).
65. R. Pennisi, J. Albanesi, P. Ascenzi, C. Nervi, A. di Masi, Are DNA damage response kinases a target for the differentiation treatment of acute myeloid leukemia? *IUBMB Life* **70**, 1057–1066 (2018).
66. M. A. Santos *et al.*, DNA-damage-induced differentiation of leukaemic cells as an anti-cancer barrier. *Nature* **514**, 107–111 (2014).
67. S. A. Gatz *et al.*, Phase I/II study of the PARP inhibitor olaparib and ATR inhibitor ceralasertib in children with advanced malignancies: Arm N of the AcSé-ESMART trial [abstract]. *Cancer Res.* **83** (suppl. 8), CT019 (2023).
68. V. Sundararajan *et al.*, Nuclear pCHK1 as a potential biomarker of increased sensitivity to ATR inhibition. *J. Pathol.* **259**, 194–204 (2023).
69. T. F. Eleveld *et al.*, Relapsed neuroblastomas show frequent RAS–MAPK pathway mutations. *Nat. Genet.* **47**, 864–871 (2015).
70. E. W. Deutsch *et al.*, The ProteomeXchange consortium at 10 years: 2023 update. *Nucleic Acids Res.* **51**, D1539–D1548 (2023).
71. Y. Perez-Riverol *et al.*, The PRIDE database resources in 2022: A hub for mass spectrometry-based proteomics evidences. *Nucleic Acids Res.* **50**, D543–D552 (2022).